Journal of Power Sources 243 (2013) 225–232

Contents lists available at SciVerse ScienceDirect

Journal of Power Sources

journal homepage: www.elsevier.com/locate/jpowsour

Enhancement of activity of $RuSe_x$ electrocatalyst by modification with nanostructured iridium towards more efficient reduction of oxygen

Beata Dembinska [a], Malgorzata Kiliszek [a], Hanna Elzanowska [a], Marcin Pisarek [b], Pawel J. Kulesza [a,*]

[a] Department of Chemistry, University of Warsaw, Pasteura 1, PL-02-093 Warsaw, Poland
[b] Institute of Physical Chemistry, Polish Academy of Sciences, Kasprzaka 44/52, 01-224 Warsaw, Poland

HIGHLIGHTS

- Catalytic system containing carbon-supported $RuSe_x$ and Ir nanoparticles for oxygen reduction.
- Enhancement of performance of carbon-supported $RuSe_x$ for electroreduction of oxygen.
- High activity of nanostructured iridium toward decomposition of H_2O_2.
- Selectivity of iridium-decorated carbon-supported $RuSe_x$ in the presence of methanol.

ARTICLE INFO

Article history:
Received 30 January 2013
Received in revised form
3 May 2013
Accepted 23 May 2013
Available online 6 June 2013

Keywords:
Oxygen reduction
Hydrogen peroxide
Acid electrocatalysis
Ruthenium–selenium nanoparticles
Nanostructured iridium
Bifunctional mechanism

ABSTRACT

Electrocatalytic activity of carbon (Vulcan XC-72) supported selenium-modified ruthenium, $RuSe_x$/C, nanoparticles for reduction of oxygen was enhanced through intentional decoration with iridium nanostructures (dimensions, 2–3 nm). The catalytic materials were characterized in oxygenated 0.5 mol dm^{-3} H_2SO_4 using cyclic and rotating ring disk voltammetric techniques as well as using transmission electron microscopy and scanning electron microscopy equipped with X-ray dispersive analyzer. Experiments utilizing gas diffusion electrode aimed at mimicking conditions existing in the low-temperature fuel cell. Upon application of our composite catalytic system, the reduction of oxygen proceeded at more positive potentials, and higher current densities were observed when compared to the behavior of the simple iridium-free system ($RuSe_x$/C) investigated under the analogous conditions. The enhancement effect was more pronounced than that one would expect from simple superposition of voltammetric responses for the oxygen reduction at $RuSe_x$/C and iridium nanostructures studied separately. Nanostructured iridium acted here as an example of a powerful catalyst for the reduction of H_2O_2 (rather than O_2) and, when combined with such a moderate catalyst as ruthenium–selenium (for O_2 reduction), it produced an integrated system of increased electrocatalytic activity in the oxygen reduction process. The proposed system retained its activity in the presence of methanol that could appear in a cathode compartment of alcohol fuel cell.

1. Introduction

Fuel cell research aiming at development of alternative sources of electrochemical energy has attracted significant interest during recent years. Among the applicable systems, hydrogen–oxygen and methanol–oxygen low-temperature polymer-membrane fuel cells are presently the best known and, probably, the most promising options. While oxidation of hydrogen is highly efficient and can be readily achieved at noble metal electrocatalysts, utilization of alcohol fuels for anodic reactions, though more complex, has some advantages related to their easy storage and handling. In any case, the practical efficiency of the cathodic reaction (oxygen reduction) is far from being satisfactory, and there is still need to develop new systems or to optimize the existing catalytic materials. In addition to the general problem of formation of the undesirable hydrogen peroxide intermediate and appearance of the negative potential shifts during oxygen reduction, in the case of direct alcohol fuel cells, transfer of alcohol fuel through the membrane from anodic to cathodic compartment leads to a serious interference at Pt-based electrocatalysts: overlapping of the oxygen reduction currents

* Corresponding author. Tel.: +48 22 8220211x289; fax: +48 22 8225996.
E-mail address: pkulesza@chem.uw.edu.pl (P.J. Kulesza).

0378-7753/$ – see front matter © 2013 Published by Elsevier B.V.
http://dx.doi.org/10.1016/j.jpowsour.2013.05.120

with those originating from the alcohol oxidation thus resulting in decrease of the cell voltage. In this respect, recent attempts to fabricate new catalysts that are not only highly reactive but also selective towards oxygen reduction are fully justified. For example, the systems utilizing ruthenium nanoparticles modified with submonolayers of selenium, $RuSe_x$ [1–6] can be viewed as promising alternatives to Pt-based catalysts. The $RuSe_x$ type systems tend to reduce oxygen, however, with higher overpotentials, i.e. at more negative potentials relative to the performance of standard platinum catalysts and, therefore, there is a need to search for means of enhancing their activities.

Iridium is one of the most corrosion-resistive noble metals [7] although it shows high affinity to OH and O groups. Because its surface oxidation occurs at much lower potentials relative to Pt or Au [8], it is likely that this phenomenon is responsible for lower reactivity of iridium (in comparison to platinum) for the oxygen reduction [7]. It has been postulated [9] that while preanodization of Ir lowers its electrocatalytic activity towards oxygen reduction, it enhances its reactivity towards the reductive hydrogen peroxide decomposition. Further, iridium does not effectively electrocatalyze oxidations of alcohols including methanol in acid media [10,11]. The latter phenomenon favors its use as a component of the cathode catalytic material for use in direct alcohol fuel cells. It has also been observed that interfacial modification of metallic iridium nanoparticles with selenium leads to the enhancement of Ir activity towards oxygen reduction as well as to improvement of the system's tolerance to the presence of methanol in supporting electrolyte [10,11]. In this respect, specific interactions, involving electronic transfers between Ir and Se has been postulated. The $IrSe_x$ nanoparticles have occurred to be particularly active when stabilized with Nafion [12,13]. In a few papers it was also suggested that iridium oxides, bare and modified with other transition metals, are effective catalysts of oxygen reduction [14–16]. It is noteworthy that doping of iridium with certain transition metals such as Ru, Mo, W or V leads to the enhancement of its activity [15]. There are also some reports indicating improvement of the electrocatalytic activity of platinum towards oxygen reduction by alloying it with iridium [17,18]. It is not clear whether the enhancement originated from the electronic interactions between Pt and Ir, the interfacial competition between the metals' OH adsorbates leading to the hindrance of the OH_{ads} formation on the neighboring Pt atoms or reactivity of Ir itself.

When it comes to the hydrogen peroxide reduction, the process was found to be somewhat more effective (at least in neutral media) [19] on metallic iridium rather than on iridium covered by the electrochemically generated oxide layers presumably due to relatively poor conductivity of iridium (III) oxides. It was also postulated that the porous structure favored penetration of H_2O_2 at the Ir/IrOx interface [19] as well as that the Ir-oxide redox species [20–22] were found to be particularly involved in the hydrogen peroxide reduction. The overall high activity of iridium structures (Ir and IrOx) towards H_2O_2 reduction (or oxidation) was utilized for detection of H_2O_2 produced in the course of enzymatic reactions [23,24]. The system's electrocatalytic activity was even further enhanced when iridium species were combined with ruthenium or palladium [25].

In the present work, we explore the ability of iridium nanostructures of 2–3 nm dimensions to effectively decompose, i.e. reduce readily at fairly high potentials (in acid medium) hydrogen peroxide that typically appears as undesirable intermediate during reduction of oxygen in fuel cells. When iridium nanostructures are combined with a catalyst of moderate activity, such as carbon-supported $RuSe_x$ nanoparticles, a highly reactive composite system for the oxygen reduction is produced. Another important issue is that, by analogy to bare $RuSe_x$ and regardless the addition of iridium, the composite system did not diminish its activity in the presence of methanol that could appear in the cathodic compartment of a real alcohol polymer-membrane low-temperature fuel cell.

2. Experimental

The electrochemical measurements were performed with CH Instruments (Austin, TX, USA) Model 750A and 600B workstations. A saturated calomel electrode (SCE) with potential 0.25 V more positive relative to the reversible hydrogen electrode (RHE) was used as a reference electrode. All potentials are expressed against the reversible hydrogen electrode (RHE). Voltammetric and rotating ring disk electrode (RRDE) voltammetric experiments were accomplished using a variable speed rotator (Pine Instruments, USA). The electrode assembly utilized a glassy carbon disk and Pt ring. The geometric area of the disk electrode was 0.166 cm^2. The collection efficiency of the RRDE assembly, determined according to procedure described before [1], was equal to 0.23. During the RRDE experiments in oxygen saturated solutions, the potential of the ring electrode was kept at 1.2 V vs. RHE. At this potential, any H_2O_2 generated at the disk was oxidized under convection–diffusional control. The electrodes were polished with aqueous alumina slurries (grain size, 5–0.05 μm) on a Buehler polishing cloth.

The activity of examined catalysts was also tested with use of home-made gas diffusion electrode (geometric area of active part, 1 cm^2) mounted into a Teflon holder with provision for oxygen feeding from the back of the electrode. A Pt ring served as a current collector. The commercial teflonated carbon paper in the form of circle with geometric area of 1.33 cm^2 (Toray carbon paper EC-TP1-060T; thickness, 190 μm) was modified by dropping with the micropipette 100 μl volume of inks prepared according to the procedures described below. The electrodes were dried in air atmosphere and at room temperature (20 °C) for 2 h.

All chemicals were commercial materials of the highest available purity (ACS reagent grade). The solution of 5% Nafion-1100 was from Aldrich. As a rule solutions were prepared from triply-distilled subsequently-deionized water. They were de-aerated (using nitrogen) or saturated with oxygen at least 30 min prior to the electrochemical measurements. Experiments were conducted at room temperature (about 25 °C).

Carbon (Vulcan XC-72) supported $RuSe_x$ clusters were fabricated using the procedure analogous to that proposed earlier at Helmholtz–Zentrum–Berlin, Germany [26]. Their composition was as follows: Ru – 20%, Se – 1% and C – 79% (by mass).

The sol solution of iridium nanoparticles was prepared as described earlier [27,28]. 0.2 g of sodium ethoxide was dissolved in 6 ml of absolute ethanol by stirring in a 100 mL round bottom flask. $IrCl_3$ (in molar ratio to sodium ethoxide 1–3) was added and the solution was refluxed under Ar for ca. 2 h. After cooling down to room temperature the mixture was stirred under Ar for ca. 20 h, and finally filtered through fine filter paper (Qualitative, Whatman). The Ir sol filtrate was used for further experiments. To perform electrochemical experiments, 3 μl of the suspension properly diluted with ethanol (in volume ratio 1:10) was introduced onto the surface of GC electrode and then dried in air at room temperature for 48 h.

To produce an ink of bare $RuSe_x$/C nanoparticles, 5 mg of the catalyst was dispersed in 200 μl of ethanol, and subjected mixing at magnetic stirrer for 1 h. Then 80 μl of the 5% Nafion solution in the mixture of lower aliphatic alcohols and water (from Aldrich) was added and suspension was subjected mixing at magnetic stirrer for several hours. The ink of iridium-modified $RuSe_x$/C was produced in an analogous manner but before Nafion was added, $RuSe_x$/C nanoparticles had been mixed with 28 μl of the sol–gel solution of nanostructured iridium for ca. 10 h. As a rule, a known volume of

aliquot of the appropriate ink (3 μl) was introduced onto the surface of rotating disc electrode. Obtained loading of Ru was about 65 μg cm^{-2} for $RuSe_x$/C ink and about 60 μg cm^{-2} for $RuSe_x$/C-Ir ink. The electrodes were air-dried at room temperature. The catalytic films were activated by performing 20–30 full voltammetric potential cycles in the potential range from 0 to 0.9 V (at 50 mV s^{-1}) until steady-state currents were observed.

The morphology of catalytic particles was monitored using Philips CM 10 transmission electron microscope (TEM) operating at 100 kV and Carl Zeiss scanning electron microscope (SEM). To estimate the atomic ratio of Ru to Ir, the energy dispersive X-ray analysis (EDAX) was conducted.

X-ray photoelectron spectroscopy (XPS) measurements were accomplished with Microlab 350 spectrometer having the maximum energy resolution 0.83 eV while using Al K_α non-monochromatic radiation (1486.6 eV, 300 W) as the exciting source. The pressure during analysis was 5.0×10^{-9} Pa. The measured binding energies were corrected by referring to the energy of C 1s at 284.5 eV as the internal standard. XPS spectra were fitted with use of Avantage 4.16 XPS software for data acquisition and processing.

3. Results and discussion

Fig. 1 illustrates TEM images of (a) carbon-supported $RuSe_x$ ($RuSe_x$/C), (b) nanostructured iridium, and (c) $RuSe_x$/C admixed or modified with iridium nanostructures. The dark spots of dimensions of a few nm can be attributed to both $RuSe_x$ and Ir nanoparticles. The greyish structures of sizes of 20–40 nm should be referred to carbon supports. It seems that $RuSe_x$ nanoparticles have diameters of 4–7 nm (Fig. 1a), and they tend to be attached tightly to carbon supports. Iridium nanostructures (Fig. 1b) are even smaller (2–3 nm), which is in agreement with previously reported data [27], and they are dispersed homogenously over $RuSe_x$/C (Fig. 1c).

EDAX spectrum of the Ir-modified $RuSe_x$/C suspended within the ink containing Nafion gave the following chemical compositions (in at%): Ru 1.2%, Se 0.1%, C 74% and Ir 0.7%. The analytical data were also consistent with the presence of oxygen as well as certain amounts of fluorine and sulfur most probably originating from Nafion binder. The molar ratio between the two most important elements, Ru-to-Ir, was 1.7–1 (their weight ratio was equal to 0.9–1). When calculated versus the geometric electrode surface area, the iridium loading was equal 67 μg cm^{-2}. Considering the amounts of chemicals used for the iridium sol synthesis relative to the added $RuSe_x$/C catalyst, molar ratio of Ru-to-Ir should be equal 2 to 1 (while the weight ratio is 1.1 to 1). This result is in good agreement with the data obtained from EDAX analysis.

We have performed XPS measurements to comment on the chemical identity of iridium nanostructures. Deconvolution of the Ir-4f spectrum characteristic of the as-prepared sample (i.e. investigated just after washing with distilled water) shows two doublets (Fig. 2a). The binding energies for the first doublet (the most intensive) are 60.8 and 63.8 eV, and the data correspond to $4f_{7/2}$ and $4f_{5/2}$ lines of metallic iridium, respectively. Quantitative analysis is consistent with the view that approximately 80% of the as-prepared sample is in metallic form. When the experiments have been repeated with the samples subjected to potential cycling (between

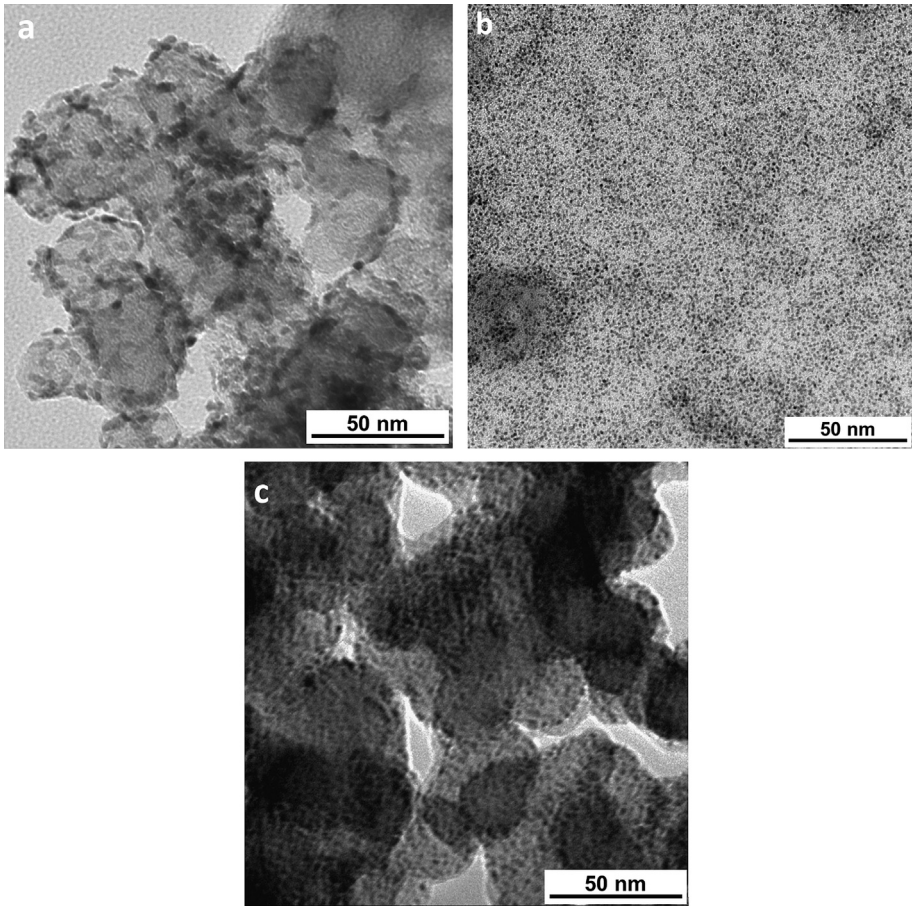

Fig. 1. TEM images of (a) $RuSe_x$/C, (b) nanostructured iridium and (c) iridium-modified $RuSe_x$/C nanoparticles.

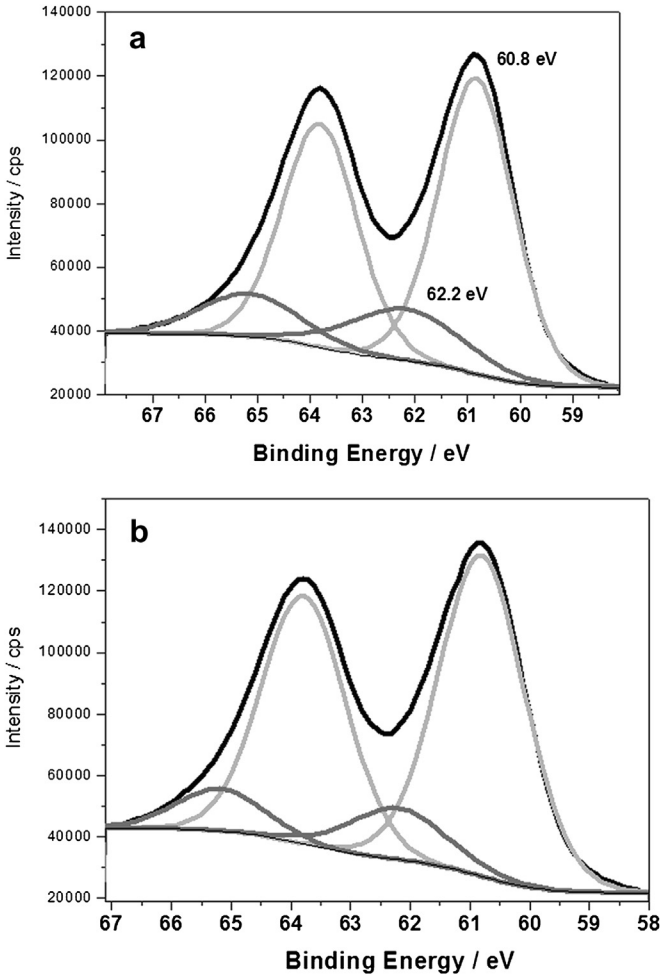

Fig. 2. XPS spectra of the Ir 4f region recorded for the nanostructured iridium supported on glassy carbon substrate: (a) as-prepared sample, and (b) investigated following potential cycling up to 0.9 V.

0 and 0.9 V for 30 min), the amount of metallic iridium has increased to about 85% (Fig. 2b). The origin of the pair of peaks appearing at 62.2 and 65.2 eV is unclear. They may be attributed to the presence of Ir(I) or to the interactions of iridium with chlorine and sodium that may exist as traces in the sample [29]. In addition there was no shift in O1s spectrum characteristic for oxides or hydroxides of transition metals; the binding energies for the O1s spectrum (observed at 532.6 and 534.7 eV) should be attributed to C—O bondings existing on the glassy carbon substrate [29]. Although our iridium nanostructures seem to be predominantly metallic, the XPS results cannot reflect the real characteristics of the iridium surface (which has high affinity to OH and O groups [8,9]) under conditions of an electrochemical experiment in sulfuric acid, where iridium becomes readily covered by various oxo species.

Cyclic voltammetric responses of (a) $RuSe_x$/C, (b) nanostructured iridium, and (c) $RuSe_x$/C modified with iridium nanostructures are shown in Fig. 3. While the voltammogram of bare $RuSe_x$/C catalyst is characterized by a fairly flat background currents (curve a) because hydrogen adsorption/desorption peaks of metallic ruthenium are suppressed following modification with selenium [2], the Ir-modified system (curve c) has exhibited fairly high voltammetric currents at potentials lower than 0.3 V. They should be attributed to the presence of nanostructured iridium. Indeed, the cyclic voltammogram of iridium deposited onto glassy carbon electrode and investigated in the deaerated 0.5 mol dm^{-3} H_2SO_4 (curve b) has

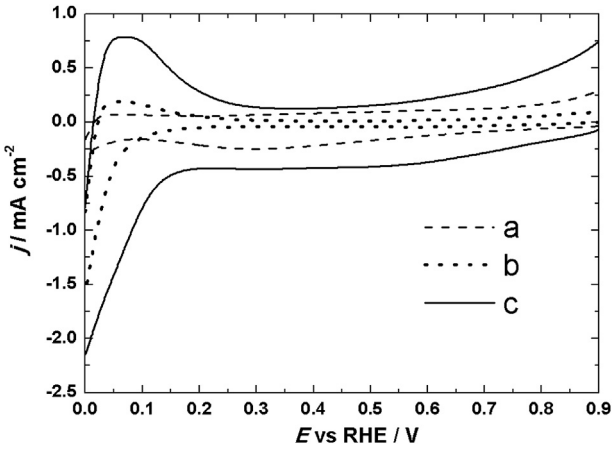

Fig. 3. Cyclic voltammetric responses of the following catalytic systems: (a) $RuSe_x$/C, (b) nanostructured iridium and (c) iridium-modified $RuSe_x$/C nanoparticles deposited onto a glassy carbon electrode substrate. Electrolyte: nitrogen saturated 0.5 mol dm^{-3} H_2SO_4. Scan rate: 5 mV s^{-1}.

yielded characteristic hydrogen adsorption/desorption peaks at potentials below 0.3 V [27]. Because of electroactivity of iridium direct comparison of voltammetric currents, appearing at bare $RuSe_x$/C and upon introduction of iridium is not straightforward. Therefore, we cannot conclude that, as before in the case $RuSe_x$/C modified with ultra-thin films of tungsten oxide [1,30], the $RuSe_x$ currents are suppressed. In the present voltammetric study, we do not have any direct evidence for the formation of iridium oxo-species but, as already mentioned, metallic iridium has high tendency to generate surface OH or O groups at low potentials, namely just above the region of adsorption/desorption of atomic hydrogen [8,9].

Fig. 4 illustrates capacitive background-subtracted voltammetric curves recorded in the oxygen saturated electrolytes for the following electrocatalytic systems deposited on glassy carbon: (a) $RuSe_x$/C, (b) nanostructured iridium, and (c) $RuSe_x$/C modified with iridium nanostructures. Comparison of results in Fig. 4 leads to the conclusion that, under voltammetric conditions of Fig. 4, the iridium-modified $RuSe_x$/C system is characterized by the highest oxygen reduction currents and the peak appearing at the most positive potential (0.730 V in curve c), in comparison to the performance of single component systems, nanostructured iridium (curve b) and $RuSe_x$/C (curve a). It is noteworthy that the nanostructured iridium itself has behaved as not a powerful catalyst for

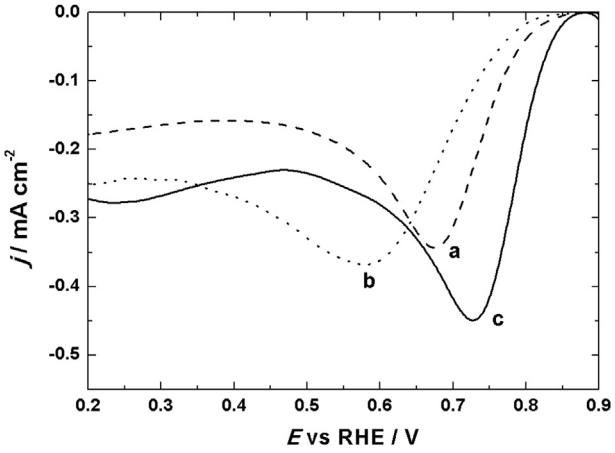

Fig. 4. Background-subtracted voltammetric responses for the reduction of oxygen at (a) $RuSe_x$/C, (b) nanostructured iridium and (c) iridium-modified $RuSe_x$/C nanoparticles. Electrolyte: O_2-saturated 0.5 mol dm^{-3} H_2SO_4. Scan rate: 5 mV s^{-1}.

oxygen reduction and yielded the voltammetric peak (curve b) at potentials ca. 100 mV more negative than that characteristic of $RuSe_x/C$ (curve a). On the other hand, modification of $RuSe_x/C$ with nanostructured iridium results in shifting the oxygen reduction potential ca. 50 mV towards more positive values (compare curves a and c).

Further diagnosis of the systems' electrocatalytic performance was done using rotating ring disk electrode (RRDE) voltammetry. Fig. 5 illustrates the normalized (capacitive background-subtracted) responses recorded at the disk electrode at 1600 rpm for (a) $RuSe_x/C$, (b) nanostructured iridium, and (c) $RuSe_x/C$ modified with iridium nanostructures. The results are in agreement with the voltammetric data of Fig. 4 clearly indicating the highest electrocatalytic activity of the iridium-modified $RuSe_x/C$ system (curve c). Also under rotating disk conditions, Ir nanostructures could only reduce oxygen at potentials lower than ca. 0.75 V. To determine kinetic parameters (that will be discussed later), the disk currents were recorded at different rotation rates; for simplicity we only show in inset to Fig. 5 the data for the optimum iridium-modified $RuSe_x/C$ system.

To obtain quantitative information about the relative formation of H_2O_2 (X_{H2O2} in %) during the reduction of oxygen under the RRDE voltammetric conditions the assembly with Pt ring was used. Curves a, b and c in Fig. 6 refer to the ring responses recorded for $RuSe_x/C$, nanostructured iridium and iridium-modified $RuSe_x/C$ nanoparticles, respectively. The highest ring currents have been observed and, consequently, the largest absolute amounts of hydrogen peroxide are produced in the potential range from 0.7 to 0.1 V. In a case of the bare iridium catalyst, formation of hydrogen peroxide has significantly decreased (curve b in Fig. 6). We also compare the H_2O_2 ring (oxidation) currents to the oxygen reduction disk currents and comment on the relative formation of hydrogen peroxide. The % amounts of H_2O_2 were calculated from the data of Figs. 5 and 6 by using equation described earlier [31–33]:

$$X_{H_2O_2} = \frac{200 I_R/N}{I_D + I_R/N} \quad (1)$$

where I_R is ring current, I_D stands for disk current and N is the collection efficiency of the RRDE assembly. Results of the $X_{H_2O_2}$ determinations are presented in the inset of Fig. 6 and are plotted versus potential applied to the disk electrode. At potentials more positive than 0.7 V, the oxygen reduction currents recorded at disk

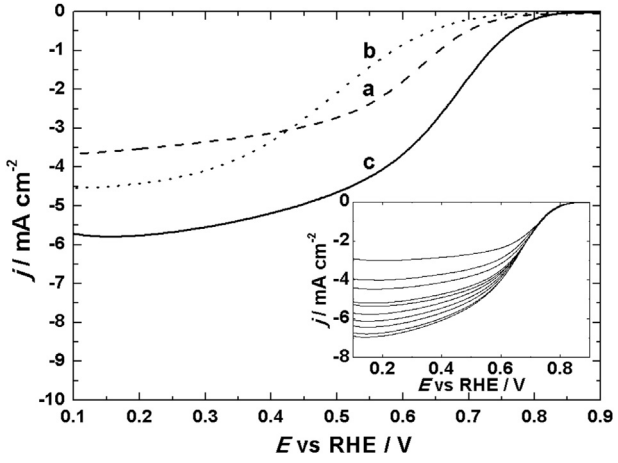

Fig. 5. Normalized (background subtracted) rotating disk voltammograms for oxygen reduction at (a) $RuSe_x/C$, (b) nanostructured iridium and (c) Ir-modified $RuSe_x/C$ nanoparticles. Rotation rate, 1600 rpm. Other conditions as for Fig. 4. Inset shows RDE voltammograms for oxygen reduction at iridium-modified $RuSe_x/C$ recorded at different rotation rates (ranging from 400 to 2500 rpm).

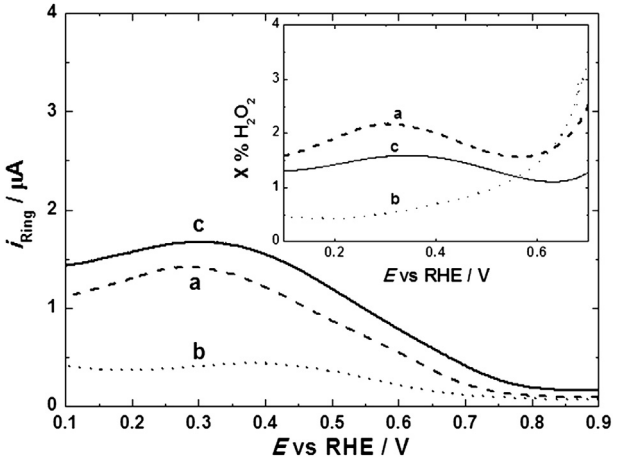

Fig. 6. Currents recorded at Pt ring and calculated fraction of hydrogen peroxide (X $\%_{H2O2}$) (inset) produced during reduction of oxygen under conditions of RRDE voltammetric experiments of Fig. 5 for the following catalytic systems: (a) $RuSe_x/C$, (b) nanostructured iridium and (c) Ir-modified $RuSe_x/C$ nanoparticles.

electrode (particularly for $RuSe_x/C$ and nanostructured Ir) are not well-developed because the applied potential is not sufficiently negative to drive effectively the ORR; consequently, the results of ring measurements are largely uncertain. Thus we have decided to limit our considerations about the fraction of hydrogen peroxide ($X_{H_2O_2}$) formed to the potential range from 0.1 to 0.7 V. At the glassy carbon disk electrode modified with the ink of Ir-admixed $RuSe_x/C$ nanoparticles (curve c), the production of H_2O_2 has been found definitely the lowest, relative to the single component systems, $RuSe_x/C$ (curve a) and nanostructured iridium (curve b), at potentials higher than 0.55 V. On the other hand, the system utilizing nanostructured iridium only (curve b) has produced the lowest percentage amount of hydrogen peroxide at potentials more negative than 0.55 V. At this stage, we believe that our system is not optimized yet, and we have not attempted to discuss possible mechanisms proposed for oxygen reduction on platinum [34,35].

When the disk current densities (recorded in the oxygen saturated solutions and measured at 0.6 V) were plotted versus the square root of the rotation rate (for simplicity not shown here), the deviation from linearity (i.e., from the ideal behavior characteristic for systems limited solely by convective diffusion of oxygen in the solution) was more pronounced at bare $RuSe_xC$ rather than the Ir-modified system. Apparently, the electrocatalytic reduction of oxygen proceeded more effectively at iridium-modified $RuSe_x/C$. In the next step, on the basis of so-called Koutecky–Levich reciprocal plots (Fig. 7), we estimated heterogeneous rate constants for examined systems from the following dependence [36]:

$$\frac{1}{I_{lim}} = \frac{1}{nFAkC_{film}C_{O_2}} + \frac{1}{I_d} \quad (2)$$

where I_{lim} stood for the limiting current measured, I_d was the ideal convective-diffusional current described according to the Levich equation, k was rate constant of the catalytic reaction (in homogeneous units), F stood for the Faraday constant, C_{film} was the surface concentration of the catalytic sites, C_{O2} was the bulk (solution) concentration of oxygen (ca. 1.1 mmol dm^{-3} in 0.5 mol dm^{-3} H_2SO_4 [37]), and n was the number of electrons involved in the process. Here we made the assumption that only such factors as transport of oxygen in solution, or at higher rotation rates, the dynamics of the catalytic reaction were rate-determining steps. From the intercepts of Koutecky–Levich reciprocal plots (Fig. 7), the values of kC_{film}, which are equivalent to the heterogeneous rate

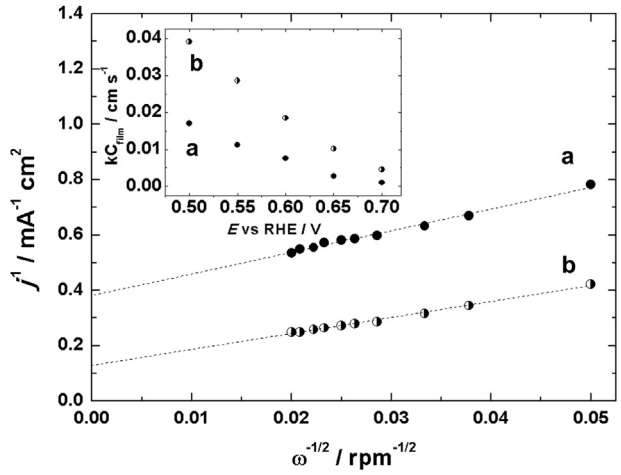

Fig. 7. Koutecky–Levich reciprocal plots for the electroreduction of oxygen at 0.6 V and dependencies (inset) of the related heterogeneous rate constants (kC_{film}) plotted as function of the potential applied to disk electrode containing (a) $RuSe_x$/C and (b) Ir-modified $RuSe_x$/C nanoparticles.

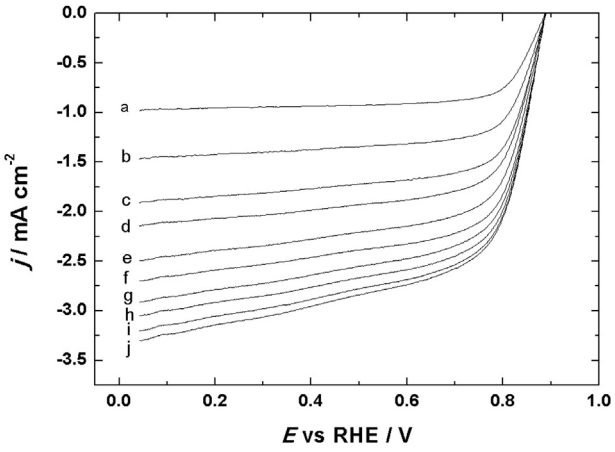

Fig. 8. Normalized (background-subtracted) rotating disk voltammetric responses for the reduction of hydrogen peroxide (2 mmol dm^{-3}) recorded at glassy carbon electrode modified with nanostructured iridium. Rotation rates: (a) 195, (b) 390, (c) 708, (d) 911, (e) 1202, (f) 1601, (g) 1850, (h) 2105 and (i) 2506 rpm. Electrolyte: deaerated 0.5 mol dm^{-3} H_2SO_4. Scan rate: 10 mV s^{-1}.

constants, were determined. They were equal to 1.8×10^{-2} and 0.8×10^{-2} cm s^{-1} for the oxygen electroreduction (at 0.6 V) at the nanostructured iridium-modified $RuSe_x$/C and bare $RuSe_x$/C, respectively. Thus, admixing of $RuSe_x$/C nanoparticles with Ir nanostructures resulted in a more than two-fold increase of the heterogeneous rate constant at examined potential. The ratio of rate constants is even higher at 0.7 V (inset to Fig. 7) and reaches the value of 4 in favor of the iridium-modified electrocatalyst. For bare iridium nanostructures, determination of kC_{film} was not possible before reaching the potential of about 0.4 V (where kC_{film} was 1.4×10^{-2} cm s^{-1}).

The observed enhancement effect and the ability of the iridium-modified system to produce less hydrogen peroxide at fairly high potentials (where nanostructured iridium itself was not very active towards the reduction of oxygen) require some attention. Among possible explanations, the existence of activating interactions between catalytic components and/or specific reactivity towards the H_2O_2 intermediate can be envisioned.

In this context, we have considered and evaluated nanostructured iridium as a potential catalyst for the hydrogen peroxide reduction. Fig. 8 illustrates the respective current-potential curves recorded at different rotation rates in the de-aerated electrolyte containing 2 mmol dm^{-3} of H_2O_2 at a glassy carbon disk modified with nanostructured iridium. It is noteworthy that reductive decomposition of H_2O_2 proceeds readily at the examined catalytic system, and the reaction occurs at more positive potentials in comparison to oxygen reduction (Figs. 4 and 5). It seems that a number of parameters, including the nanostructured character of iridium particles (i.e. their small dimensions of 2–3 nm leading to the high catalytic surface area) and perhaps existence of some interfacial iridium-oxo species (in addition to iridium in predominantly metallic form) [9] explains the system's superior activity toward H_2O_2 (rather than O_2) reduction. On the basis of data presented in Fig. 8, we have plotted Koutecky–Levich dependencies (for simplicity not shown here) and estimated heterogeneous rate (kC_{film}) constants: they are on the level of $2–4 \times 10^{-2}$ cm s^{-1} in the range of potentials from 0.7 down to 0.1 V (Table 1). It is noteworthy that the rate for hydrogen peroxide reduction is high even at such a positive potential as 0.7 V. Thus it is reasonable to expect that addition of nanostructured iridium to $RuSe_x$/C catalyst would enhance reductive decomposition of H_2O_2 and, consequently, lead to increase of the O_2-reduction current density (Fig. 5).

The overall enhancement effect (and the lowering of the hydrogen peroxide formation) can be explained in terms of the classical concepts of multi-step electrode reactions [38,39]. Here it can be envisioned that the electroreduction of oxygen proceeding to hydrogen peroxide (at $RuSe_x$ centers) can be followed by the catalytic reduction of H_2O_2 to water (at nanostructured iridium sites). Alternatively, the reduction of oxygen could proceed in two steps because the second reduction step appears at more positive potentials, i.e. it is thermodynamically more favorable than the first one [38]. Indeed, it is apparent, upon comparison of Figs. 5 and 8, that reduction of hydrogen peroxide starts at the catalytic system utilizing nanostructured iridium (Fig. 8) at almost 200 mV more positive potentials when compared to the behavior of oxygen at the film containing $RuSe_x$/C only (Fig. 5a). In this respect, the nanostructured iridium seems to be a more promising component for admixing with $RuSe_x$/C than the previously reported tungsten oxide [30,40,41]. Another important issue is the dynamics of the second step [38,39] (e.g. reductive decomposition of H_2O_2). For well-behaved systems, the half-wave potentials could shift even a few hundred mV towards positive values provided that rate constants of the second step are as high as $10^5–10^8$ mol^{-1} dm^3 s^{-1}.

Finally, we also performed additional diagnostic experiments, namely galvanodynamic measurements with use of so-called gas diffusion electrode (GDE) operating under conditions resembling those characteristic of the cathode in a real fuel cell. Fig. 9 shows typical polarization (potential vs. flowing current) curves recorded in the oxygen saturated 1 mol dm^{-3} H_2SO_4 following application of different catalytic systems, conventional $RuSe_x$/C (solid line, curve a) and $RuSe_x$/C modified with nanostructured iridium (solid line, curve b). It is apparent that, for the same current densities applied,

Table 1
The dependence of heterogeneous rate constant of hydrogen peroxide reduction on potential for Ir nanoparticles.

E vs RHE/V	10^2 kC_{film}/cm s^{-1}
0.1	4.5
0.2	3.9
0.3	3.5
0.4	3.1
0.5	2.8
0.6	2.5
0.7	2.2

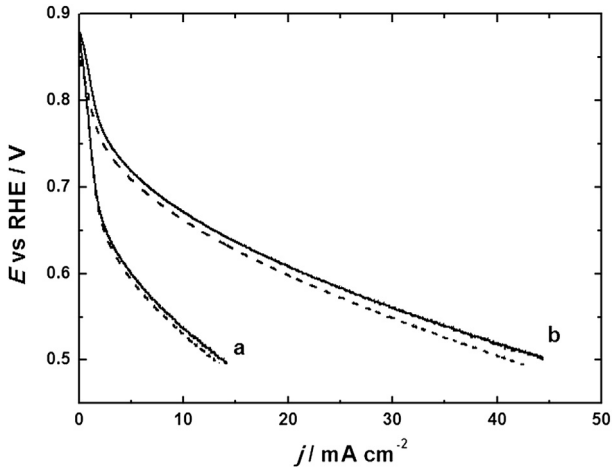

Fig. 9. Galvanostatic steady-state polarization curves recorded for the oxygen reduction at (a) bare $RuSe_x$/C and (b)Ir-modified $RuSe_x$/C nanoparticles in the absence (solid lines) and presence (dashed lines) of 0.5 mol dm^{-3} CH_3OH. Oxygen flux: 100 ml min^{-1}; temperature: 25 °C; electrolyte: oxygen saturated 1 mol dm^{-3} H_2SO_4; loading of Ru: 0.27 mg cm^{-2} for $RuSe_x$/C and 0.24 mg cm^{-2} for Ir-modified $RuSe_x$/C nanoparticles.

higher half-cell potentials were observed for the iridium-modified system. When the analogous experiments were repeated in the presence of 0.5 mol dm^{-3} methanol (to mimic the situation of the possible methanol crossover to the cathode compartment in a real fuel cell), the behavior of both catalytic systems was almost unchanged (dashed lines) in comparison to that obtained in pure electrolyte (solid lines).While the methanol tolerance of such a catalyst as $RuSe_x$ (during oxygen reduction) is well-established [1,2,42], an important observation is that admixing and utilization of nanostructured iridium (contrary to platinum) does not change this characteristics. Probably, the presence of selenium in close vicinity of iridium nanoparticles hinders the activity of the latter element towards methanol oxidation, what is in agreement with literature data [10].

4. Conclusions

Addition of iridium nanoparticles to $RuSe_x$/C catalyst results in the enhancement of its performance during the electroreduction of oxygen in acid medium. This effect is demonstrated in terms of the higher catalytic current densities observed, shifting the oxygen reduction potential towards more positive values and approximately two-fold increase of the heterogeneous rate constant measured at 0.6 V. Another issue of importance to the technology of alcohol fuel cells is that the iridium-decorated $RuSe_x$/C is selective towards oxygen reduction in the presence of such an organic fuel as methanol.

The electrocatalytic enhancement effect was more pronounced than that one would expect from summing up of activities of single components, namely simple $RuSe_x$/C and iridium nanostructures considered separately. The observed synergism may be explained in terms of the bifunctional nature of the composite catalytic system in which $RuSe_x$/C induces reduction of oxygen whereas any undesirable hydrogen peroxide intermediate products may be readily decomposed (reduced) at dispersed iridium acting as a highly reactive and specific catalyst in the latter case. Regardless the actual mechanism, an important practical issue is that the relative amounts of hydrogen peroxide (generated during reduction of oxygen at potentials higher than 0.55 V) are much lower at iridium-modified $RuSe_x$/C in comparison to bare $RuSe_x$/C nanoparticles. In this respect, high activity of nanostructured iridium towards decomposition of the undesirable intermediate (H_2O_2) even at such a positive potential as 0.7 V should be mentioned. Although we do not have sufficient evidence yet, the existence of stabilizing interactions between nanostructured iridium and $RuSe_x$, analogous to those previously postulated for the tungsten oxide modified $RuSe_x$ systems [30,40,41], is also very likely here.

Finally, the nanostructured iridium utilized here is not a practical catalyst for fuel cells because of its high cost. But the present observations (implying the enhancement effect following introduction of a model catalyst highly active toward hydrogen peroxide in addition to the system's tolerance to methanol) could be of general importance to the fuel cell research. In this respect, behavior of iridium is different than that of platinum. Indeed, addition of nanostructured Pt to $RuSe_x$ does not lead to any enhancement effect (for simplicity the results are not shown here); moreover, Pt becomes largely passivated presumably by interacting with selenium present on ruthenium.

Acknowledgments

The support from National Science Centre (Poland) under grant N N204 269840 is highly appreciated. This work was also supported in part from Foundation for Polish Science (FNP) under Chair (Mistrz) Program. We are grateful to Krzyszt of Miecznikowski and Karolina Malinowska for their technical assistance during transmission electron microscopy experiments.

References

[1] A. Kolary-Zurowska, A. Zieleniak, K. Miecznikowski, B. Baranowska, A. Lewera, S. Fiechter, P. Bogdanoff, I. Dorbandt, R. Marassi, P.J. Kulesza, J. Solid State Electrochem. 11 (2007) 915–921.
[2] D. Cao, A. Wieckowski, J. Inukai, N. Alonso-Vante, J. Electrochem. Soc. 153 (2006) A869–A874.
[3] D.C. Papageorgopoulos, F. Liu, O. Conrad, Electrochim. Acta 52 (2007) 4982–4986.
[4] A.K. Shukla, R.K. Raman, K. Scott, Fuel Cells 05 (2005) 436–447.
[5] T.J. Schmidt, U.A. Paulus, H.A. Gasteiger, N. Alonso-Vante, R.J. Behm, J. Electrochem. Soc. 147 (2000) 2620–2624.
[6] N. Alonso-Vante, Pure Appl. Chem. 80 (2008) 2103–2114.
[7] D.A.J. Rand, R. Woods, J. Electroanal. Chem. 55 (1974) 375–381.
[8] J. Mozota, B.E. Conway, Electrochim. Acta 28 (1983) 1–8.
[9] J.P. Hoare, J. Electroanal. Chem. 18 (1968) 251–259.
[10] K. Lee, L. Zhang, J. Zhang, J. Power Sources 165 (2007) 108–113.
[11] K. Lee, L. Zhang, J. Zhang, J. Power Sources 170 (2007) 291–296.
[12] Y. Zhang, H. Zhang, Y. Zhang, Y. Ma, H. Zhong, H. Ma, Chem. Commun. (2009) 6589–6591.
[13] T. Xu, H. Zhang, Y. Zhang, H. Zhong, H. Jin, Y. Tang, J. Power Sources 196 (2011) 5849–5852.
[14] Y. Takasu, N. Yoshinaga, W. Sugimoto, Electrochem. Commun. 10 (2008) 668–672.
[15] N. Yoshinaga, W. Sugimoto, Y. Takasu, Electrochim. Acta 54 (2008) 566–573.
[16] C.H. Chang, T.S. Yuen, Y. Nagao, H. Yugami, J. Power Sources 195 (2010) 5938–5941.
[17] T. Ioroi, K. Yasuda, J. Electrochem. Soc. 152 (2005) A1917–A1924.
[18] M.B. Vukmirovic, J. Zhang, K. Sasaki, A.U. Nilekar, F. Uribe, M. Mavrikakis, R.R. Adzic, Electrochim. Acta 52 (2007) 2257–2263.
[19] H. Elzanowska, E. Abu-Irhayem, B. Skrzynecka, V.I. Birss, Electroanalysis 16 (2004) 478–490.
[20] J.A. Cox, R.K. Jaworski, Anal. Chem. 61 (1989) 2176–2178.
[21] J.A. Cox, R.K. Jaworski, J. Electroanal. Chem. 281 (1990) 163–170.
[22] R.K. Jaworski, J.A. Cox, B.R. Strohmeier, J. Electroanal. Chem. 325 (1992) 111–123.
[23] F. Tian, G. Zhu, Sensors Actuators B 86 (2002) 266–270.
[24] J. Wang, G. Rivas, M. Chicharro, J. Electroanal. Chem. 439 (1997) 55–61.
[25] S.A. Miscoria, G.D. Barrera, G.A. Rivas, Electroanalysis 14 (2002) 981–987.
[26] M. Bron, P. Bogdanoff, S. Fiechter, I. Dorbandt, M. Hilgendorff, H. Schleburg, H. Tributsch, J. Electroanal. Chem. 500 (2001) 510–517.
[27] V.I. Birss, H. Andreas, I. Serebrennikova, H. Elzanowska, Electrochem. Solid-State Lett. 2 (1999) 326–329.
[28] A.S. Jhasa, H. Elzanowska, B. Sebastiana, V. Birs, Electrochim. Acta 55 (2010) 7683–7689.
[29] J. Chastain, R.C. King Jr., Handbook of X-ray Photoelectron Spectroscopy, Physical Electronics Inc., 1995.
[30] A. Lewera, K. Miecznikowski, R. Hunger, A. Kolary-Zurowska, A. Wieckowski, P.J. Kulesza, Electrochim. Acta 55 (2010) 7603–7609.
[31] O. Antoine, R. Durand, J. Appl. Electrochem. 30 (2000) 839–844.

[32] H. Schulenburg, M. Hilgendorff, I. Dorbandt, J. Radnik, P. Bogdanoff, S. Fiechter, M. Bron, H. Tributsch, J. Power Sources 155 (2006) 47–51.
[33] M. Chatenet, L. Génies-Bultel, M. Aurousseau, R. Durand, F. Andolfatto, J. Appl. Electrochem. 32 (2002) 1131–1140.
[34] P.S. Ruvinskiy, A. Bonnefont, C. Pham-Huu, E.R. Savinova, Langmuir 27 (2011) 9018–9027.
[35] A. Schneider, L. Colmenares, Y.E. Seidel, Z. Jusys, B. Wickman, B. Kasemo, R.J. Behm, Phys. Chem. Chem. Phys. 10 (2008) 1931–1943.
[36] P.J. Kulesza, B. Grzybowska, M.A. Malik, M.T. Galkowski, J. Electrochem. Soc. 144 (1997) 1911–1917.
[37] N. Alonso-Vante, H. Tributsch, O. Solorza-Feria, Electrochim. Acta 40 (1995) 567–576.
[38] A.J. Bard, L.R. Faulkner, Electrochemical Methods Fundamentals and Applications, second ed., John Wiley & Sons, 2001.
[39] Z. Galus, Fundamentals of Electrochemical Analysis, second ed., Ellis Horwood and Polish Scientific Publishers, New York, Warsaw, 1994.
[40] P.J. Kulesza, K. Miecznikowski, B. Baranowska, M. Skunik, S. Fiechter, P. Bogdanoff, I. Dorbandt, Electrochem. Commun. 8 (2006) 904–908.
[41] P.J. Kulesza, K. Miecznikowski, B. Baranowska, M. Skunik, A. Kolary-Zurowska, A. Lewera, K. Karnicka, M. Chojak, I. Rutkowska, S. Fiechter, P. Bogdanoff, I. Dorbandt, G. Zehl, R. Hiesgen, E. Dirk, K.S. Nagabhushana, H. Boennemann, J. Appl. Electrochem. 37 (2007) 1439–1446.
[42] G. Zehl, P. Bogdanoff, I. Dorbandt, S. Fiechter, K. Wippermann, C. Hartnig, J. Appl. Electrochem. 37 (2007) 1475–1484.